Discovery of [11C]MK-8193 as a PET tracer to measure target engagement of phosphodiesterase 10A (PDE10A) inhibitors

Christopher D. Cox [a,*], Eric D. Hostetler [b], Broc A. Flores [a], Jeffrey L. Evelhoch [b], Hong Fan [b], Liza Gantert [b], Marie Holahan [b], Waisi Eng [b], Aniket Joshi [b], Georgia McGaughey [c], Xiangjun Meng [b], Mona Purcell [b], Izzat T. Raheem [a], Kerry Riffel [b], Youwei Yan [d], John J. Renger [e], Sean M. Smith [e], Paul J. Coleman [a]

[a] Discovery Chemistry, Merck Research Laboratories, West Point, PA 19486, USA
[b] Imaging, Merck Research Laboratories, West Point, PA 19486, USA
[c] Chemical Modeling & Informatics, Merck Research Laboratories, West Point, PA 19486, USA
[d] Structural Chemistry, Merck Research Laboratories, West Point, PA 19486, USA
[e] Neuroscience, Merck Research Laboratories, West Point, PA 19486, USA

ARTICLE INFO

ABSTRACT

Phosphodiesterase 10A (PDE10A) inhibition has recently been identified as a potential mechanism to treat multiple symptoms that manifest in schizophrenia. In order to facilitate preclinical development and support key proof-of-concept clinical trials of novel PDE10A inhibitors, it is critical to discover positron emission tomography (PET) tracers that enable plasma concentration/PDE10A occupancy relationships to be established across species with structurally diverse PDE10A inhibitors. In this Letter, we describe how a high-throughput screening hit was optimized to provide [11C]MK-8193 (8j), a PET tracer that supports the determination of plasma concentration/PDE10A occupancy relationships for structurally diverse series of PDE10A inhibitors in both rat and rhesus monkey.

© 2015 Elsevier Ltd. All rights reserved.

Following discovery of the phosphodiesterase 10A (PDE10A) enzyme in 1999, rapid progress has been made in understanding its physiological localization and function using genetic, biologic and pharmacologic techniques.[1] Pioneering work by a group at Pfizer suggested that PDE10A inhibition may be an effective new mechanism to ameliorate the positive symptoms of schizophrenia, characterized most prominently by hallucinations and delusions.[2] Subsequent efforts from groups across the pharmaceutical industry have provided preclinical data suggesting that PDE10A inhibitors may also be effective in addressing the cognitive impairment and negative symptoms of schizophrenia, with a differentiated side-effect profile relative to currently marketed agents.[3] PDE10A inhibitors have also been proposed as potential therapeutic agents to treat Huntington's disease.[4] Consistent with the significant therapeutic potential for PDE10A inhibition, no less than 20 companies have filed patent applications on novel chemical matter for PDE10A,[3b] and at least seven of those companies have initiated clinical trials.[5]

Not surprisingly, based on a general agreement that positron emission tomography (PET) tracers can be critical components of CNS drug discovery efforts,[6] many companies and academic labs have pursued the development of PET tracers as target engagement biomarkers to establish plasma concentration/PDE10A occupancy relationships in preclinical efficacy studies and assist in dose-selection for clinical studies.[7] Multiple PDE10A tracers have provided promising results in preclinical species, and preliminary human data for several of these indicate that they should indeed allow assessment of target engagement in the human brain and enable occupancy/efficacy relationships to be established in key Phase 2 proof-of-concept studies.[7d,g–i] Preliminary evidence has been presented that suggests PDE10A PET tracers may also be valuable as diagnostic biomarkers in the early stages of Huntington's disease.[8] In this report, we describe the discovery of [11C]MK-8193 (8j), a PDE10A PET tracer derived from a Merck high-throughput screening (HTS) hit, and show its utility for measuring target engagement of PDE10A inhibitors in the rat and rhesus monkey brain.

Our initial interest in PDE10A was spurred by the pioneering work at Pfizer where highly potent and selective inhibitors such

* Corresponding author. Tel.: +1 (215) 652 2411; fax: +1 (215) 652 7310.
E-mail address: chris_cox@merck.com (C.D. Cox).

ARTICLE IN PRESS

2

C. D. Cox et al./Bioorg. Med. Chem. Lett. xxx (2015) xxx–xxx

as **MP-10** were discovered and employed to probe the biology of PDE10A inhibition in vivo.[9] Our first attempts at PET tracer development were based on incorporation of radioisotopes onto the **MP-10** scaffold to provide ligands such as **1a** and **1b** that were studied in vitro and in vivo. As others have reported,[7a–c] we found that the slow kinetics, high non-displaceable binding, and the potential to form brain-penetrant metabolites with **1a** and **1b** made these analogs less than ideal for PET tracer development;[10] however, this work was instrumental in illustrating that a useful PDE10A PET tracer was highly feasible given the density and localization of PDE10A.

MP-10

1a R = $^{11}CH_3$
1b R = $CH_2CH_2^{18}F$
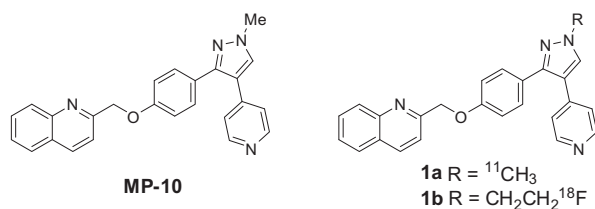
Rather than try to optimize the **MP-10** series into a suitable tracer as other groups have reported,[7b,c,f] we instead elected to progress a novel scaffold identified from our ongoing lead-finding efforts. To that end, we had earlier embarked on a broad effort to identify novel PDE10A inhibitors that included HTS, ALIS (Automated Ligand Identification System),[11] and fragment screening, and our laboratory has recently disclosed novel series of PDE10A inhibitors derived from hits identified by each of these methods: **2**, **3**, and **4**, respectively (Fig. 1).[12] An additional hit identified from HTS was quinazolinone **5**, a compound that stood out as having good potency with moderate ligand binding efficiency (LBE) and reasonable calculated properties ($c\,Log\,P$ = 3.9, PSA = 75).

Initial SAR efforts in the quinazolinone series made use of the one-pot procedure illustrated in Scheme 1 for exploration of the
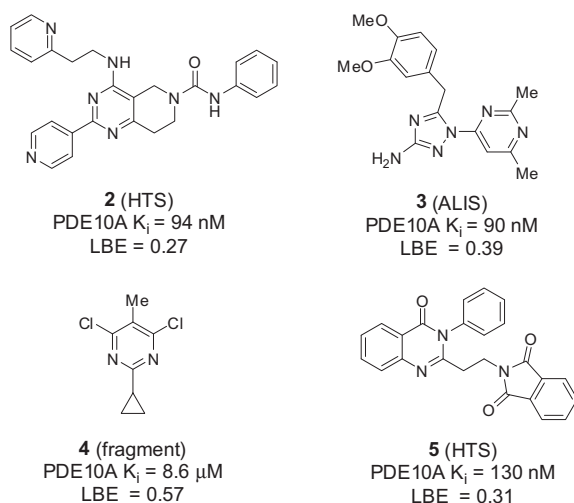

2 (HTS)
PDE10A K_i = 94 nM
LBE = 0.27

3 (ALIS)
PDE10A K_i = 90 nM
LBE = 0.39

4 (fragment)
PDE10A K_i = 8.6 μM
LBE = 0.57

5 (HTS)
PDE10A K_i = 130 nM
LBE = 0.31

Figure 1. Hits identified by internal screening at Merck.

Table 1
Initial SAR exploration of HTS hit **5**

Compound	R^1	R^2	PDE10A K_i (nM)
6a	2-Me	H	1124
6b	3-Me	H	109
6c	4-Me	H	87
6d	4-F	H	280
6e	4-Cl	H	123
6f	4-CN	H	265
6g	4-Ph	H	49
6h	4-OMe	H	61
6i	3,4-DiOMe	H	64
6j	4-OMe	1-Cl	171
6k	4-OMe	2-Cl	163[a]
6l	4-OMe	3-Cl	45
6m	4-OMe	4-Cl	>1000[a]
6n	4-OMe	3-OMe	39
6o	4-OMe	3-Me	15
7	—	—	13

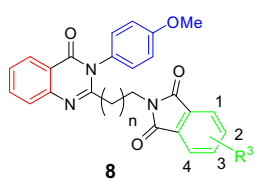[a] Represents data from a single determination.

northeastern (blue) and western (red) aryl groups. Though many additional compounds were made and tested, the progression of SAR in Table 1 highlights the salient features.[13] Compounds **6a–c** illustrate that whereas methyl substitution at the 2-position of the northeastern aryl is not tolerated, methyl substituents at the 3- or 4-positions are slightly potency enhancing, with a small advantage provided by the latter. Compounds **6d–i** indicate that whereas 4-F, 4-Cl, and 4-CN are detrimental to potency relative to 4-Me, 4-OMe and 4-Ph are potency enhancing, and disubstitution at the 3- and 4-positions is not advantageous over the monosubstituted analog (cf. **6h → 6i**). Holding the R^1 group constant as OMe and walking a chlorine atom around the western aryl ring at the R^2 position (**6j–m**) indicates that 3-substitution is optimal, with **6l** demonstrating a potency of 45 nM. Changing R^2 to a more polar 3-OMe group maintained potency, but 3-Me provided the most potent analog, **6o**, with PDE10A K_i = 15 nM (LBE = 0.33). We also explored aryl rings other than phenyl in the northeastern region, but most compounds led to a significant reduction in potency; one notable exception was indole **7** that, without the potency-enhancing R^2 substituent at the 3-position on the western aryl, provided a 14 nM inhibitor (LBE = 0.32). Though increases in activity were modest to this point, **6o** and **7** provided a nearly a 10-fold increase in potency over the HTS hit **5** while maintaining acceptable LBE and physical properties, thus providing us with inspiration to continue SAR exploration in other regions of the molecule.

With the optimal western and northeastern substitutions in hand, we then focused our attention on the phthalimide and linker region. Decreasing the linker length to one carbon (**8a**) or increasing it to three carbons (**8b**) were both detrimental to potency (Table 2), as were aliphatic substitutions on the alkyl chain (data
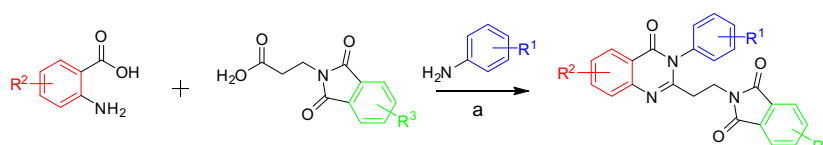
Scheme 1. Reagents and conditions: (a) P(OPh)$_3$, pyridine, 100 °C in a sealed tube; then add aniline and heat to 100 °C (yields: 25–75%).

ARTICLE IN PRESS

C. D. Cox et al. / Bioorg. Med. Chem. Lett. xxx (2015) xxx–xxx　　　　3

Table 2
Additional SAR exploration of leading quinazolinone **6h**

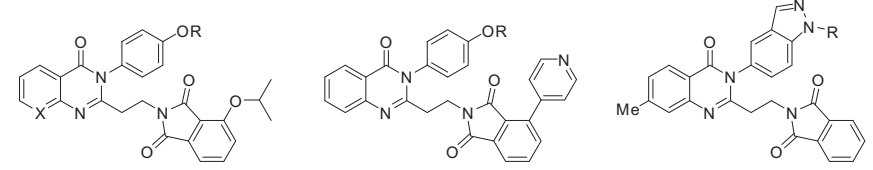| Compound	n	R^3	PDE10A K_i (nM)
8a	0	H	>1000[a]
8b	2	H	219
8c	1	1-Cl	7.7
8d	1	2-Cl	30
8e	1	1,4-DiCl	6.3
8f	1	1-Me	6.1
8g	1	1-OH	20
8h	1	1-OMe	2.0
8i	1	1-OEt	1.0
8j	1	1-OiPr	0.15
8k	1	1-Br	8.4[a]
8l	1	1-(2-Thiazole)	1.8
8m	1	1-(4-Pyridyl)	0.072

[a] Represents data from a single determination.

not shown). Most attempts to remove or alter the phthalimide group were also unsuccessful, though some efforts toward that end were fruitful and will be the subject of a future publication. However, investigating substitution around the aryl (green) ring of the phthalimide provided the key breakthrough in potency we were seeking. Compounds **8c–d** indicate that substitution at the 1-position was more favorable than the 2-position, with the 1-Cl analog demonstrating single-digit nanomolar potency for the first time (**8c**). 1,4-Dichloro substitution provided no significant improvement over monosubstitution (**8e** vs **8c**) but significantly increased lipophilicity. Altering 1-Cl to 1-Me was potency neutral (**8f**), but the corresponding phenol **8g** resulted in a 3-fold loss in activity. However, using the phenol as a synthetic handle to examine various alkoxy groups at the 1-position illustrated that increased potency can be had by increasing the size of the substituent (**8h–j**), with the isopropyl analog **8j** providing the first sub-nanomolar

PDE10A inhibitor in this series with K_i = 150 pM (LBE = 0.37). Installation of a 1-bromo substituent to provide **8k** was potency neutral with respect to the 1-Cl analog **8c**, but provided a convenient handle for installation of aryl substituents via cross-coupling chemistry. Among the multiple 1-aryl groups installed, the 2-thiazole (**8l**) and the 4-pyridyl (**8m**) stood out as two of the most interesting in terms of potency and drug-like properties.

At this point in our exploration of the quinazolinones, we noted that although the pharmacokinetics of leading compounds was uniformly poor, with clearance in rat being near hepatic blood flow, the rest of the profile looked favorable as illustrated in Table 3 for the most potent analogs described thus far, **8j** and **8m**. These compounds have: (1) improved LBE's relative to HTS hit **5**, (2) HPLC Log$D$s in a drug-like range,[14] (3) high selectivity for PDE10A over the other PDEs; (4) moderate plasma protein binding; (5) no Pgp efflux liability in human or rat, and (6) very good cellular permeability. These characteristics, along with being highly amenable to radiolabel incorporation at the phenolic methyl ether, made them ideal candidates to investigate as potential PET tracers. At this point, two additional compounds were rationally designed as potential PET tracers for in vivo analysis: (1) compound **9**, incorporating a nitrogen at the 8-position of the quinazolinone core, was made in an effort to further reduce the lipophilicity of **8j**, and (2) compound **10**, the most potent analog identified within this series, which was made based on indole **7**, but incorporating an additional nitrogen to form an indazole system which lowered lipophilicity relative to the corresponding indole analog.

The four compounds illustrated in Table 3 were radiolabeled with ^{11}C and studied in vivo in rhesus monkey to assess brain uptake and specific binding to PDE10A. Somewhat surprisingly, compound **8j** which, based on in vitro data looked less promising than the others based on its intermediate potency and higher HPLC Log$D$,[15] was the standout in terms of in vivo profile with high brain uptake, rapid washout, and a very large apparent signal.[16] A baseline PET image of [^{11}C]**8j** in rhesus monkey brain is shown in Figure 2A. As expected based on the distribution of PDE10A in the brain, highest tracer uptake was observed in the striatum with very low tracer retention in all other brain regions. Striatal uptake in rat brain was lower than in rhesus monkey, but rapid washout in regions devoid of PDE10A result in a useful specific signal (Fig. 3A).

Table 3
In vitro characterization of leading tracer candidates

8j R = CH₃; X = CH
[^{11}C]-**8j** R = [11]CH₃; X = CH

9 R = CH₃; X = N
[^{11}C]-**9** R = [11]CH₃; X = N

8m R = CH₃
[^{11}C]-**8m** R = [11]CH₃

10 R = CH₃
[^{11}C]-**10** R = [11]CH₃

	8j	9	8m	10
PDE10A K_i (nM)	0.15	0.37	0.072	0.025
LBE	0.37	0.35	0.36	0.37
HPLC Log$D$ (pH 7)	3.6	2.8	2.8	3.4
PDE selectivity[a]	>60,000	>27,000	>29,000	>100,000
Protein binding (human) (%)	97	83	93	98
Pgp (B-A/A-B)	⩽1	⩽1	⩽1	⩽1
Permeability ($\times10^{-6}$ cm/s)	28	39	31	27

[a] PDE selectivity is calculated by the following formula: PDEX K_i/PDE10A K_i wherein PDEX is the PDE other than PDE10A with the most potent K_i.
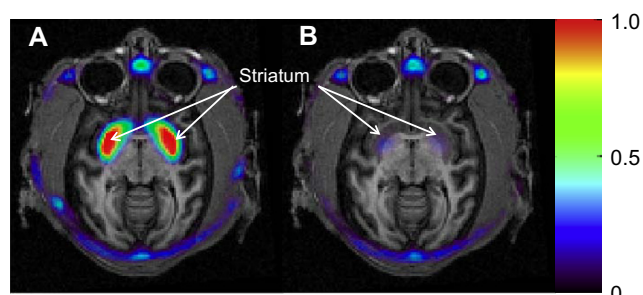
ARTICLE IN PRESS

4   C. D. Cox et al. / Bioorg. Med. Chem. Lett. xxx (2015) xxx–xxx

Figure 2. Summed PET images (30–90 min) of [^{11}C]**8j** in rhesus monkey brain overlaid on MRI under baseline conditions (A) and after administration of THPP-1 (B). The baseline PET study shows high tracer retention (red color) in the striatum. Tracer binding in the striatum is blocked after administration of THPP-1. Scale is in SUV (standardized uptake value).
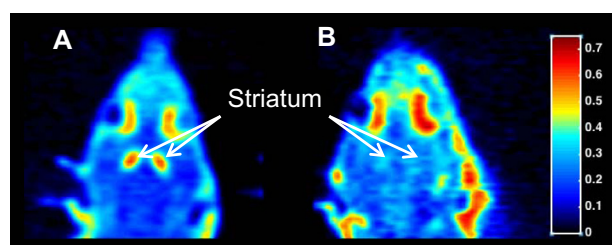

Figure 3. Summed PET images (0–90 min) of [^{11}C]**8j** in rat brain under baseline conditions (A) and after administration of THPP-1 (B). The baseline PET study shows high tracer retention (red color) in the striatum. Tracer binding in the striatum is blocked after administration of THPP-1. Scale is in SUV (standardized uptake value).

In contrast to the excellent in vivo rhesus monkey data for [^{11}C]**8j**, [^{11}C]**8m** displayed high non-specific binding and a possible brain-penetrant metabolite in rhesus, while [^{11}C]**9** had a smaller specific signal relative to [^{11}C]**8j**, despite having similar potency with more drug-like physicochemical properties (lower HPLC Log*D* and greater free fraction in plasma). The most potent compound, [^{11}C]**10**, provided a very large signal in vivo, but was slow to reach steady-state, making occupancy determinations less certain. We also studied several ^{11}C-labeled analogs from the THPP series (derived from HTS hit **2**) in vivo in rhesus monkeys that had in vitro profiles nearly identical to that of **8j**; however, these tracers uniformly displayed poor brain uptake for reasons that are not completely understood. The uncertainty of translation from in vitro predictions to in vivo behavior underscores the advantages of having an embedded imaging chemist on a project team with resources to study multiple promising compounds in vivo.[17]

The synthetic route utilized to provide [^{11}C]**8j** is highlighted in Scheme 2.[18] The 1-isopropoxyphthalimide intermediate **13** was made via a three-step procedure starting with **11**, and then coupled via the one-pot procedure described in Scheme 1 to provide benzyl-protected phenol **14**. Removal of the benzyl group with TMSBr in TFA with thioanisole provided the labeling precursor **15**. Synthesis of [^{11}C]**8j** was carried out in good yield with high specific activity (>1 Ci/μmol) and purity using [^{11}C]CH$_3$I and Cs$_2$CO$_3$ in DMF.

With a robust route available to access quantities of [^{11}C]**8j** on demand, we proceeded to study its utility for evaluating target engagement of a leading series of PDE10A inhibitors in rat and rhesus monkey brain. Figure 2 shows a summed PET image of [^{11}C]**8j** in rhesus monkey both at baseline and after a 15 mpk iv dose of the PDE10A inhibitor **THPP-1**.[12a] The markedly reduced tracer retention in the striatum after THPP-1 administration indicates the ability of [^{11}C]**8j** to determine PDE10A occupancy for this structurally diverse PDE10A inhibitor. Similar results were observed in the rat brain at baseline and after a 6 mpk i.v. dose of **THPP-1**, as illustrated in Figure 3. A forthcoming publication will demonstrate the usefulness of [^{11}C]**8j** for determining quantitative plasma exposure/PDE10A occupancy relationships in both rat and rhesus monkey striatum, as well as provide data that support the expectation that [^{11}C]**8j** will also provide a useful specific signal in humans.[19,20]
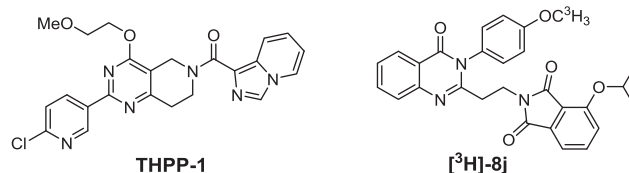
Importantly for our preclinical development program, a tritiated version of **8j**, [^{3}H]**8j**, was found to be a useful tracer for establishing a high-throughput, ex vivo occupancy assay in the rat, and future publications from our group will demonstrate how this assay allowed us to drive lead optimization efforts based on maximizing PDE10A occupancy in the brain while minimizing plasma exposure. It is important to note that, as illustrated in Figures 2 and 3, [^{11}C]**8j** is able to determine PDE10A occupancy of compounds from series that are structurally diverse from the tracer itself. In fact, during the course of our program, we have investigated the ability of [^{11}C]**8j** and [^{3}H]**8j** to determine plasma/occupancy correlations across many structurally diverse series of PDE10A inhibitors, including the THPPs, leads derived from ALIS hit **3** and fragment
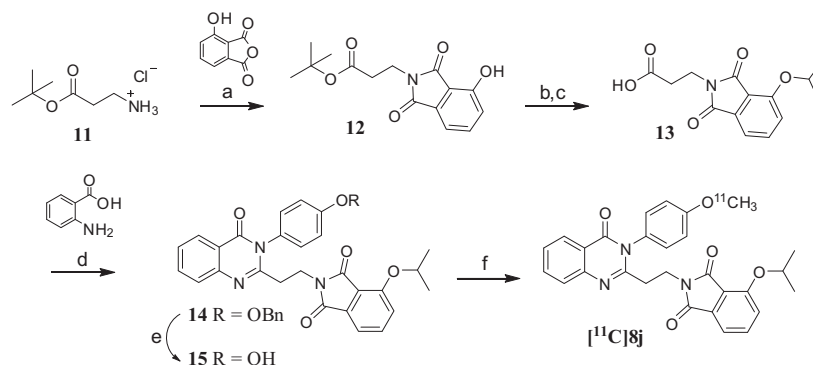
Scheme 2. Reagents and conditions: (a) dioxane, triethylamine, 50 °C (65% yield); (b) Cs$_2$CO$_3$, *i*PrI, CH$_3$CN, 40 °C; (c) TFA, DCM (75% for 2 steps); (d) P(OPh)$_3$, pyridine, 100 °C in a sealed tube; then *p*-OBn aniline (78% yield); (e) TMSBr, TFA, thioanisole, 0 °C (64% yield); (f) [^{11}C]CH$_3$I, Cs$_2$CO$_3$, DMF, 45 °C, 3 min.

ARTICLE IN PRESS

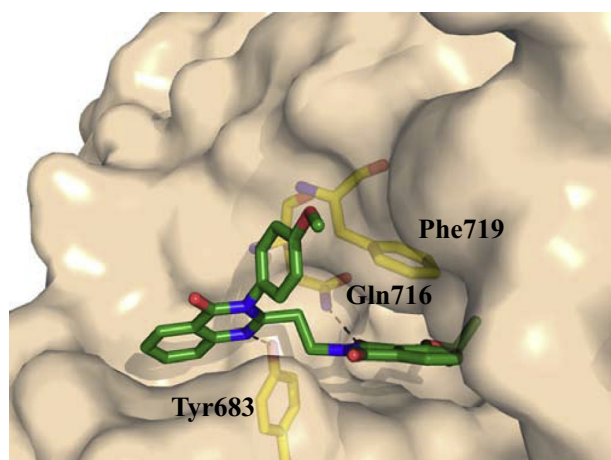*C. D. Cox et al./Bioorg. Med. Chem. Lett. xxx (2015) xxx–xxx*

5

Figure 4. X-ray of **8j** in the PDE10A enzyme active site. Key residues and hydrogen-bonding interactions are highlighted.

hit **4**, as well as **MP-10** itself; in every case, the tracer allowed us to determine plasma/PDE10A occupancy relationships and enable cross-compound, cross-series and cross-species comparisons.

The ability of [^{11}C]**8j** to determine occupancy across multiple series of PDE10A inhibitors can be readily explained by examining the X-ray crystal structure of **8j** bound to the PDE10A catalytic core domain as shown in Figure 4.[21] As expected, the tracer binds in the active site and forms direct interactions with key active site residues: One phthalimide oxygen is engaged in a hydrogen bonding interaction (d_{N-O} = 3.2 Å) with the conserved Gln 716, the phthalimide aryl group engages in a π-stacking interaction with Phe 719, and the quinazolinone ring fills the PDE10A 'selectivity pocket' with the nitrogen at the 1-position of the ring engaged in a hydrogen-bonding interaction (d_{N-O} = 2.7 Å) with Tyr-683. Notably, all reported PDE10A inhibitors have been found to bind in this same region of the enzyme and make at least two of these three key interactions, nicely explaining the utility of **8j** to enable occupancy measurement across many diverse series of PDE10A inhibitors.

Based on the results of in vitro and in vivo studies, some of which were shown herein, as well as additional favorable characteristics such as safety, selectivity, pharmacokinetics, metabolism profile, and pharmaceutical properties, [^{11}C]**8j** was selected for development as a target engagement biomarker to support development of PDE10A inhibitors and identified as [^{11}C]**MK-8193**. Forthcoming reports will provide a more detailed characterization of the in vitro and in vivo behavior of this tracer, and demonstrate how it was used to drive our lead optimization program.

Acknowledgments

References and notes

1. Chappie, T. A.; Helal, C. J.; Hou, X. *J. Med. Chem.* **2012**, *55*, 7299.
2. (a) Menniti, F. S.; Chappie, T. A.; Humphrey, J. M.; Schmidt, C. J. *Curr. Opin. Invest. Drug* **2007**, *8*, 54; (b) Schmidt, C. J.; Chapin, D. S.; Cianfronga, M. L.; Corman, M. L.; Hajos, M.; Harms, J. F.; Hoffman, W. E.; Lebel, L. A.; McCarthy, S. A.; Nelson, F. R.; Proulx-LaFrance, C.; Majchrzak, M. J.; Ramirez, A. D.; Schmidt, K.; Seymour, P. A.; Siuciak, J. A.; Tingley, F. D., III; Williams, P. R.; Verhoest, P. R.; Menniti, F. S. *J. Pharmacol. Exp. Ther.* **2008**, *325*, 681.
3. (a) Grauer, S. M.; Pulito, V. L.; Navarra, R. L.; Kelly, M. P.; Kelley, C.; Graf, R.; Langen, B.; Logue, S.; Brennan, J.; Jiang, L.; Charych, E.; Engerland, U.; Liu, F.; Marquis, K. L.; Malamas, M.; Hage, T.; Comery, T. A.; Brandon, N. J. *J. Pharmacol. Exp. Ther.* **2009**, *331*, 574; (b) Kehler, J.; Nielsen, J. *Curr. Pharm. Des.* **2011**, *17*, 137; (c) Smith, S. M.; Uslaner, J. M.; Cox, C. D.; Huszar, S. L.; Cannon, C. E.; Vardigan, J. D.; Eddins, D.; Toolan, D. M.; Kandebo, M.; Yao, L.; Raheem, I. T.; Schreier, J. D.; Breslin, M. J.; Coleman, P. J.; Renger, J. J. *Neuropharmacology* **2013**, *64*, 215; (d) Nawrocki, A. R.; Rodriguez, C. G.; Toolan, D. M.; Price, O.; Henry, M.; Forrest, G.; Szeto, D.; Keohane, C. A.; Pan, Y.; Smith, K. M.; Raheem, I. T.; Cox, C. D.; Hwa, J.; Renger, J. J.; Smith, S. M. *Diabetes* **2014**, *63*, 300.
4. (a) Kleiman, R. J.; Kimmel, L. H.; Bove, S. E.; Lanz, T. A.; Harms, J. F.; Romegialli, A.; Miller, K. S.; Willis, A.; Des-Etages, S.; Kuhn, M.; Schmidt, C. J. *J. Pharmacol. Exp. Ther.* **2011**, *336*, 64; (b) Giampà, C.; Laurenti, D.; Anzilotti, S.; Bernardi, G.; Menniti, F. S.; Fusco, F. R. *PLoS One* **2010**, *5*, e13417.
5. The following companies have publically announced clinical trials with their associated PDE10A inhibitors: Pfizer (PF-254590), Amgen (AMG 579), Roche (RO 5545965), Lundbeck (Lu AF 11167), Takeda (TAK-063), En Vivo/Forum (EVP-6308), and Omeros (OMS824 and OMS643762).
6. Honer, M.; Gobbi, L.; Martarello, L.; Comley, R. *Drug Discovery Today* **2014**, *19*, 1936.
7. (a) Tu, Z.; Fan, J.; Li, S.; Jones, L. A.; Cui, J.; Padakanti, P. K.; Xu, J.; Zeng, D.; Shoghi, K. I.; Perlmutter, J. S.; Mach, R. H. *Bioorg. Med. Chem.* **2011**, *19*, 1666; (b) Andrés, J.-I.; De Angelis, M.; Alcàzar, J.; Iturrino, L.; Langlois, X.; Dedeurwaerdere, S.; Lenaerts, I.; Vanhoof, G.; Celen, S.; Bormans, G. *J. Med. Chem.* **2011**, *54*, 5820; (c) Celen, S.; Koole, M.; Ooms, M.; DeAngelis, M.; Sannen, I.; Cornelis, J.; Alcazar, J.; Schmidt, M.; Verbruggen, A.; Langlois, X.; VanLaere, K.; Andrés, J. I.; Bormans, G. *NeuroImage* **2013**, *82*, 13; (d) Van Laere, K.; Ahmad, R. U.; Hudyana, H.; Dubois, K.; Schmidt, M. E.; Celen, S.; Bormans, G.; Koole, M. *J. Nucl. Med.* **2013**, *54*, 1285; (e) Hwang, D.-R.; Hu, E.; Rumfelt, S.; Easwaramoorthy, B.; Castrillon, J.; Davis, C.; Allen, J. R.; Chen, H.; Treanor, J.; Abi-Dargham, A.; Slifstein, M. *Nucl. Med. Biol.* **2014**, *41*, 343; (f) Ooms, M.; Celen, S.; Koole, M.; Langlois, X.; Schmidt, M.; DeAngelis, M.; Andrés, J. I.; Verbruggen, A.; Van Laere, K.; Bormans, G. *Nucl. Med. Biol.* **2014**, *41*, 695; (g) Plisson, C.; Weinzimmer, D.; Jakobsen, S.; Natesan, S.; Salinas, C.; Lin, S.-F.; Labaree, D.; Zheng, M.-Q.; Nabulsi, N.; Marques, T. R.; Kapur, S.; Kawanishi, E.; Saijo, T.; Gunn, R. N.; Carson, R. E.; Rabiner, E. A. *J. Nucl. Med.* **2014**, *55*, 595; (h) Barret, O.; Thomae, D.; Tavares, A.; Alagille, D.; Papin, C.; Waterhouse, R.; McCarthy, T.; Jennings, D.; Marek, K.; Russell, D.; Seibyl, J.; Tamagnan, G. *J. Nucl Med.* **2014**, *55*, 1297; (i) Kehler, J.; Kilburn, J. P.; Estrada, S.; Christensen, S. R.; Wall, A.; Thibblin, A.; Lubberink, M.; Bundgaard, C.; Brennum, L. T.; Steiniger-Brach, B.; Christoffersen, C. T.; Timmermann, S.; Kreilgaard, M.; Antoni, G.; Bang-Andersen, B.; Nielson, J. J. *J. Nucl Med.* **2014**, *55*, 1513; (j) Harada, A.; Suzuki, K.; Miura, S.; Hasui, T.; Kamiguchi, N.; Ishii, T.; Taniguchi, T.; Kuroita, T.; Takano, A.; Stepanov, V.; Halldin, C.; Kimura, H. *Nucl. Med. Biol.* **2015**, *42*, 146.
8. (a) Ahmad, R.; Bourgeois, S.; Postnov, A.; Schmidt, M. E.; Bormans, G.; Van Laere, K.; Vandenberghe, W. *Neurology* **2014**, *82*, 279; (b) Russell, D. S.; Barret, O.; Jennings, D. L.; Friedman, J. H.; Tamagnan, G. D.; Thomae, D.; Alagille, D.; Morley, T. J.; Papin, C.; Papapetropoulos, S.; Waterhouse, R. N.; Seibyl, J. P.; Marek, K. L. *JAMA Neurol.* **2014**, *71*, 1520.
9. Verhoest, P. R.; Chapin, D. S.; Corman, M.; Fonseca, K.; Harms, J. F.; Hou, X.; Marr, E. S.; Menniti, F. S.; Nelson, F.; O'Connor, R.; Pandit, J.; Proulx-LaFrance, C.; Schmidt, A. W.; Schmidt, C. J.; Suiciak, J. A.; Liras, S. *J. Med. Chem.* **2009**, *52*, 5188.
10. There has recently been some debate as to the tractability of radiolabeled analogs of **MP-10** for clinical use; see: Lin, S.-F.; Lebaree, D.; Chen, M.-K.; Holden, D.; Gallezot, J.-D.; Kapinos, M.; Teng, J.-K.; Najafzadeh, S.; Plisson, C.; Rabiner, E. A.; Gunn, R. N.; Carson, R. E.; Huang, Y. *Synapse* **2015**, *69*, 86.
11. ALIS is Merck's proprietary affinity selection-mass spectrometry (AS-MS)-based system; see: Huang, X.; Cheng, C. C.; Fischmann, T. O.; Duca, J. S.; Yang, Y.; Richards, M.; Shipps, G. W. *ACS Med. Chem. Lett.* **2012**, *2*, 123.
12. (a) Raheem, I. T.; Breslin, M. J.; Fandozzi, C.; Fuerst, J.; Hill, N.; Huszar, S.; Kandebo, M.; Kim, S. H.; Ma, B.; McGaughey, G.; Renger, J. J.; Schreier, J. D.; Sharma, S.; Smith, S. M.; Uslaner, J.; Yan, Y.; Coleman, P. J.; Cox, C. D. *Bioorg. Med. Chem. Lett.* **2012**, *22*, 5903; (b) Shipe; William, D.; Abeywickrema, P. D.; Barrow, J. C.; Bednar, R.; Bruno, J.; Cofre, V.; Coleman, P. J.; Collin, D.; Cox, C. D.; Fandozzi, C.; Getty, K.; Huszar, S.; Hutson, P.; Kemmerer, A.; Krishnan, R.; Lemaire, W.; Ma, B.; McGaughey, G.; Munshi, S.; Nguyen, S.; Nolt, M. B.; Parmentier-Batteur, S.; Raheem, I. T.; Sharik, S. S.; Sharma, S.; Smith, S. M.; Theberge, C.; Uslaner, J.; Yan, Y. *Abstracts of Papers, 247th National Meeting of the American Chemical Society, Dallas, TX*; American Chemical Society: Washington, DC, 2014. MEDI-20; (c) Cox, C. D. *Abstracts of Papers, 248th National Meeting of the American Chemical Society, San Francisco, CA*; American Chemical Society: Washington, DC, 2014. MEDI-273.
13. All PDE10A inhibitory data reported in this manuscript is the average of two or more determinations unless otherwise noted. Experimental details on the assay used to determine the K_i of PDE10A inhibition can be found in: Smith, S.

C. D. Cox et al. / Bioorg. Med. Chem. Lett. xxx (2015) xxx–xxx

M.; Uslaner, J. M.; Cox, C. D.; Huszar, S. L.; Cannon, C. E.; Vardigan, J. D.; Eddins, D.; Toolan, D. M.; Kandebo, M.; Yao, L.; Raheem, I. T.; Schreier, J. D.; Breslin, M. J.; Coleman, P. J.; Renger, J. J. *Neuropharmacology* **2013**, *64*, 215.

14. Though we use *c*Log*P* calculations in a predictive sense when designing analogs, we relied on measured HPLC Log*D* values (at pH 7) as better measure of true lipophilicity for this series because HPLC Log*D* correlated better with measured shake-flask Log*P* than did *c*Log*P*; for instance, whereas the *c*Log*P* of **8j** is 4.6, the HPLC Log*D* is 3.6 and the shake-flask Log*P* is 3.19. In general, *c*Log*P* and HPLC Log*D* show the same stack-ranking of compounds, but the absolute values of the *c*Log*P* measurements were misleadingly high.

15. Though HPLC Log*D*'s were used to monitor the optimization process, we believe shake-flask Log*P* is a better predictor of suitability for PET tracer development. With a Log*P* of 3.19, **8j** is predicted to have lipophilicity supportive of PET tracer development; however, it is more lipophilic than the other analogs in Table 3.

16. Based on this promising data, the ^{18}F fluoroethyl analog of **8j** was also made and studied in vivo; despite showing favorable attributes, we favored the advantages of ^{11}C over ^{18}F which include lower radiation exposure for patients and the ability to image the same patient multiple times per day to facilitate time-course occupancy studies.

17. The Amgen group has reported a high-throughput LC-MS/MS technique that allowed them to predict in vivo behavior of potential PDE10A PET tracers based on in vitro assays and led them to the discovery of a useful PET ligand, thus offering an alternative, experimental way to increase confidence in tracer discovery: Hu, E.; Biorn, C.; Lester-Zeiner, D.; Cho, R.; Rumfelt, S.; Kunz, R. K.; Nixey, T.; Michelsen, K.; Miller, S.; Shi, J.; Wong, J.; Della Puppa, G. H.; Able, J.; Talreja, S.; Hwang, D.-R.; Hitchcock, S. A.; Porter, A.; Immke, D.; Allen, J. R.; Treanor, J.; Chen, H. *J. Med. Chem.* **2012**, *55*, 4776.

18. For full synthetic details, see: Cox, C. D.; Flores, B. A.; Hostetler, E.; Fan, H. US Patent 8,846,000, 2014.

19. Hostetler, E. D.; Fan, H.; Joshi, A.; Zeng, Z.; Eng, W.; Gantert, L.; Holahan, M.; Meng, X.; Miller, P.; O'Malley, S.; Purcell, M.; Riffel, K.; Salinas, C.; Williams, M.; Smith, S. M.; Coleman, P. J.; Cox, C. D.; Flores, B. A.; Raheem, I. T.; Cook, J. J.; Evelhoch, J. L. *for submission to Mol. Imaging Biol.*

20. Scientists at Molecular Neuroimaging, LLC (New Haven, CT) have recently reported human clinical data with [^{18}**F**]**MNI-659**, a very close analog of [^{11}**C**]**8j**, and found it to be an excellent radiotracer for quantifying PDE10A in humans, consistent with our predictions; see Refs. 6,8b.

21. Coordinates have been deposited with RCSB Protein Data Bank (PDB) under the deposition number **4ZO5**.